Linear stability analysis of a vertically oscillated granular layer

C. Bizon, M. D. Shattuck, and J. B. Swift
Center for Nonlinear Dynamics and Department of Physics, University of Texas, Austin, Texas 78712
(Received 24 May 1999)

We present a linear stability analysis of an oscillating granular layer, treating it as an isothermal incompressible fluid with zero surface tension, which undergoes periodic collisions with and separations from an oscillating plate. Because the viscosity of the granular layer is unknown, we use the experimental value of the critical acceleration for the transition from a flat to patterned layer as input for the theory, and use the analysis to calculate the granular viscosity and the wavelength of the most unstable mode. The wavelength compares favorably with the experimental pattern wavelength. Further, we find that the wavelengths are controlled by the viscosity of the granular layer. [S1063-651X(99)11112-7]

PACS number(s): 45.70.Mg, 45.70.Qj, 47.20.−k, 05.20.Dd

I. INTRODUCTION

Dissipative systems that undergo instabilities from uniform to patterned states when driven from equilibrium are ubiquitous [1]. When oscillated vertically, both a layer of liquid and a layer of macroscopic grains will undergo an instability from a flat upper surface to a pattern of subharmonic standing waves at a critical value of the vertical acceleration [2,3]. In each case, observed patterns include stripes, squares [4,2,5,6], hexagons [2,5,6], and localized patterns [7–9]. The instability of the shaken liquid layer, called the Faraday instability, can be theoretically attacked through a linear stability analysis of the Navier-Stokes equations [10,11], yielding critical accelerations and pattern wavelengths in excellent agreement with experiment, [10–12]. A number of models have been proposed for the oscillated granular layer [13–15], but their ad hoc nature makes quantitative comparison to experiment difficult.

The pattern wavelength as a function of frequency has been experimentally measured [4,16,3,17] in the granular system, as shown in Fig. 1. Only the theory by Eggers and Riecke [18] has been able to produce results that compare well with experiment, but the equations that they use are phenomenological, and contain a surface diffusion term that has no clear physical analog.

Although some of the phenomenology of Faraday patterns and the patterns in granular media are similar, several significant differences make analysis of the granular system difficult. Collisions between individual grains, unlike the analogous collisions between molecules of the liquid, are strongly inelastic and purely repulsive. Surface tension, which acts along with gravity as a restoring force for Faraday waves, is absent in granular waves. Because neither surface tension nor air pressure hold the granular layer to the oscillating plate, the plate accelerates away from the layer whenever the plate's acceleration is downward and larger than the acceleration due to gravity, g. At a subsequent time, the free-falling layer collides sharply with the plate. Figure 2 displays a time series of this motion, as seen in molecular dynamics simulations, which agree with experimental results for the types and wavelengths of patterns obtained [19,20]. In contrast to this sequence of free flights alternating with violent collisions, a liquid layer remains in contact with the plate even for accelerations of over $10g$ [12,21]. For the granular layer, each plate-layer collision excites random motion of the grains, called granular temperature in analogy to random molecular motion; inelasticity of granular collisions subsequently damps this motion. Therefore, unlike the temperature of the liquid, the granular temperature varies both spatially and temporally. The liquid layer is incompressible; the granular layer changes in volume throughout the cycle. Finally, the variations in density and temperature lead to variations in the thermal conductivity and viscosity [22–27], or to variation in the transport of granular temperature and momentum through the medium.

Furthermore, the continuum equations of motion for granular fluids lack the stature of the analogous Navier-Stokes equations, which describe the motion of molecular fluids. The granular continuum equations have been derived from kinetic theory only in the limit of small inelasticity [28,23,24,29,30], and have been subjected to very few experimental [31–33] or numerical tests [34,35,27]. However, the striking similarity to Faraday waves suggests that an analysis similar to that for Faraday waves would be fruitful. Further, the fact that secondary instabilities of stripe patterns in the granular layer are the same as those seen in continuum systems [20] and the finding from simulations that the particle velocity distributions are nearly Gaussian [36] both argue in favor of a continuum description.

We report on a linear stability analysis of a simplified version of the granular continuum equations of motion. To produce a tractable problem, we consider only the most important of the differences between oscillated liquids and granular media. In particular, we shall examine the linear stability of an isothermal, incompressible fluid with zero surface tension, but which is allowed to leave and recollide with the oscillating plate. While the variations in granular temperature and density are bound to play a role, only the strength and timing of collisions, as incorporated into a model that treats the layer as a single inelastic ball, have been demonstrated to play a role in the stability of the flat layer [2]. Further, the reductions outlined allow us to appropriate the method that Kumar and Tuckerman [10] and Kumar [11] applied to the Faraday instability. Our analysis follows that of Ref. [11] closely, except that we allow the acceleration felt by the layer to be a more complicated func-

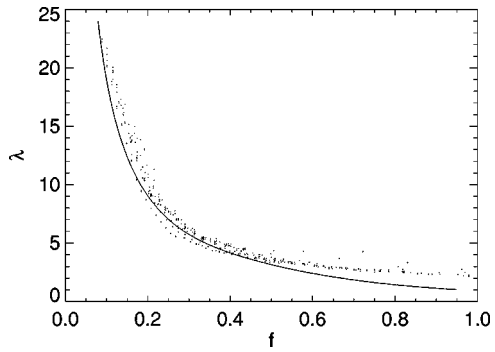

FIG. 1. Nondimensionalized wavelength versus frequency for experiment [17] above onset (dots) and the prediction of linear stability theory (line) assuming that the critical acceleration for the onset of waves is $2.5g$. The experimental data are for bronze spheres with diameter 0.165 mm and layer depths between 3 and 30 particle diameters.

tion of time than the $\cos(\omega t)$ that is appropriate for Faraday waves.

II. DEFINITION OF THE MODEL

With the assumptions that particles are nearly elastic and that single particle distribution functions are nearly Gaussian, kinetic theory has been used to derive continuum equations of motion for rapidly flowing granular media from the Boltzmann-Enskog equation for inelastically colliding hard spheres [28,23,24,30]:

$$\frac{\partial \rho'}{\partial t'} + \boldsymbol{\nabla}' \cdot (\rho' \mathbf{u}') = 0, \tag{1}$$

$$\rho' \frac{\partial \mathbf{u}'}{\partial t'} + \rho' \mathbf{u}' \cdot \boldsymbol{\nabla}' u' = -\boldsymbol{\nabla}' \cdot \underline{P}' + \mathbf{G}'(t'), \tag{2}$$

$$\rho' \frac{\partial T'}{\partial t'} + \rho' \mathbf{u}' \cdot \boldsymbol{\nabla}' T' = -\boldsymbol{\nabla}' \cdot \mathbf{q}' - \underline{\mathbf{P}}' : \underline{\mathbf{E}}' - \gamma', \tag{3}$$

where ρ' is the mass density, $\mathbf{u}'$ is the continuum velocity, $\underline{\mathbf{P}}'$ is the pressure tensor, $\mathbf{G}'(t')$ is a time dependent external force, T' is the (granular) temperature, $\mathbf{q}'$ is the heat flux, γ' is the temperature loss rate due to inelastic collisions, and $E'_{ij} = \frac{1}{2}(\partial_i u'_j + \partial_j u'_i)$. Primed quantities are dimensional; unprimed quantities will be dimensionless. Constitutive relations for $\underline{\mathbf{P}}'$ and $\mathbf{q}'$ are given by Newton's stress law and Fourier's heat law, with dynamic viscosity $\mu'(\rho', T')$ and thermal conductivity $\kappa'(\rho', T')$ provided by kinetic theory. These transport coefficients are functions of the thermodynamic state of the layer, so they will in turn depend upon the forcing parameters; as we shall see, the same layer may have different viscosities at different frequencies. Because the equations are compressible, the pressure P' is given by an equation of state.

We simplify these equations by assuming that the granular layer is isothermal and incompressible. The assumption of constant temperature is tantamount to exactly balancing the production of temperature due to collision with the plate

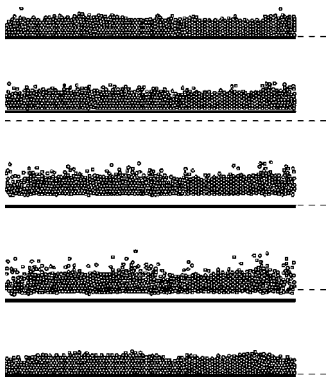

FIG. 2. This time series shows the dynamics of a granular layer over one oscillation of the plate, which is shown as a solid black bar. Each picture is separated in time by one-fourth of a period. Initially, the layer is carried upward on the moving plate. The plate then accelerates downward, leaving the layer in free fall. Finally, the layer collides with the plate and begins its upward ride. The dotted line denotes the equilibrium position of the plate. For this simulation, $\Gamma = 2.0$ and $f = 0.3$

with the loss of temperature due to inelastic collisions. In actuality, dissipation lags production, so that a large spike in the temperature occurs at each plate collision [37]. However, the duration of this large variation is only a fraction of the oscillation cycle. Similarly, the density varies slowly and the layer expands in a nearly uniform fashion in its free flight, followed by a rapid compression when the layer hits the plate. With these simplifying assumptions, and the supposition that the external force acts only in the vertical direction, the equations of motion reduce to

$$\boldsymbol{\nabla}' \cdot \mathbf{u}' = 0, \tag{4}$$

$$\rho'(\partial_{t'} \mathbf{u}' + \mathbf{u}' \cdot \boldsymbol{\nabla}' u') = -\boldsymbol{\nabla}' P' + \mu' \nabla'^2 \mathbf{u}' - G'(t') \hat{\mathbf{z}}. \tag{5}$$

We nondimensionalize the equations of motion with the depth of the layer H, the acceleration due to gravity g, and the density ρ', so that Eqs. (4) and (5) become

$$\boldsymbol{\nabla} \cdot \mathbf{u} = 0, \tag{6}$$

$$\partial_t \mathbf{u} + \mathbf{u} \cdot \boldsymbol{\nabla} \mathbf{u} = -\boldsymbol{\nabla} P + \nu \nabla^2 \mathbf{u} - G(t) \hat{\mathbf{z}}. \tag{7}$$

The nondimensional viscosity, or inverse Reynolds number, is given by $\nu = \mu' / \rho' \sqrt{H^3 g}$.

We choose a frame of reference in which the layer is at rest. Fixing $z = 0$ to the initially flat upper interface of the fluid, the base state becomes a velocity field of zero. Linearizing around this state yields

$$\boldsymbol{\nabla} \cdot \mathbf{u} = 0, \tag{8}$$

$$\partial_t \mathbf{u} = -\boldsymbol{\nabla} P + \nu \nabla^2 \mathbf{u} - G(t) \hat{\mathbf{z}}. \tag{9}$$

The function $G(t)$ here describes the effective gravity felt by the layer as it rests on the plate, flies from it, and recollides with it.

Following the fluid case, we will look for instabilities of the upper surface, which has height $\zeta(x, y, t)$. In the granular

case, we might also allow the bottom surface to go unstable, since it is free for part of each cycle. However, to simplify matters, we assume that the bottom surface stays fixed at $z=-1$. The velocity of the top surface is given by the vertical velocity component, w, at the top surface, i.e., at $z=\zeta(x,y,t)$. Taking the curl of the curl of Eq. 9 gives the equation of motion for w

$$(\partial_t-\nu\nabla^2)\nabla^2 w=0. \tag{10}$$

Note that although kinetic theory predicts $\nu(\rho,T)$, our simplifying assumptions remove ρ and T from the problem, so that we can no longer use the kinetic theory prediction to determine ν.

III. BOUNDARY CONDITIONS

For liquids, the boundary condition at $z=-1$ is no slip, since the liquid is in contact with a solid plate at all times, but for the granular case, the no-slip boundary condition is not appropriate. The granular layer leaves the plate; while the bottom surface is free, stress-free boundaries should apply. Furthermore, the interactions between fluid molecules and surfaces that produce the no-slip boundary conditions are different from the interactions between grains and the plate. Any surface is rough on the molecular level, while the plate is smooth on the scale of grains. Fluid molecules may be adsorbed onto the surface, and re-ejected with a velocity that is uncorrelated with their old velocity, but no such thermalization applies to encounters between grains and the plate. In general, granular media can exhibit a slip velocity at walls [38]; we simplify matters by assuming that at the bottom surface of the granular layer, stress free boundary conditions always apply, so that both w and $\partial_{zz}w$ equal zero at $z=-1$.

At the top surface, $\zeta(x,y,t)$, all components of the stress tensor vanish. The tangential components because they are continuous across the interface, the normal component because the surface tension of the granular layer is zero. These conditions plus incompressibility, and the assumption that the vertical velocity may be written as

$$w=w(z,t)e^{i(k_x x+k_y y)},$$

where k is the dimensionless wave number, lead to the system of equations whose stability we shall study:

$$[\partial_t-\nu(\partial_{zz}-k^2)](\partial_{zz}-k^2)w=0, \tag{11}$$

$$w|_{z=-1}=0, \tag{12}$$

$$\partial_{zz}w|_{z=-1}=0, \tag{13}$$

$$(\partial_{zz}w+k^2w)|_{z=0}=0, \tag{14}$$

$$[(\partial_t-\nu\partial_{zz}+3\nu k^2)\partial_z w]_{z=0}=k^2\zeta G(t), \tag{15}$$

$$\partial_t\zeta=w|_{z=0}. \tag{16}$$

Except for the absence of surface tension, the form of $G(t)$, and the lower boundary condition [Eq. 13)], these equations are exactly those of [11]. Equation (11) is the evolution equation for the vertical velocity, Eqs. (12) and (13) are the stress free boundary conditions at the bottom boundary, Eq. (14) is the condition on the tangential stress at the top surface, and Eq. (15) the condition on the normal stress at the top surface. Finally, Eq. (16) gives the evolution of the free surface, required for Eq. (15).

IV. FLOQUET MODES

Following [10,11], we use Floquet analysis, i.e., we assume that ζ can be written as

$$\zeta=e^{(s+i\alpha\omega)t}\sum_{n=-\infty}^{\infty}\zeta_n e^{in\omega t}, \tag{17}$$

where s and α are both real, and ω is the dimensionless angular frequency of oscillation. For harmonic response, $\alpha=0$, while for subharmonic response, $\alpha=\frac{1}{2}$.

Assuming that w can be similarly expanded, Eq. (16) gives a relation between the w_n and ζ_n, namely that

$$w_n|_{z=0}=[s+i(\alpha+n)\omega]\zeta_n. \tag{18}$$

The evolution equation [Eq. (11)] becomes an equation for each w_n,

$$(\partial_{zz}-k^2)(\partial_{zz}-q_n^2)w_n(z)=0, \tag{19}$$

$$q_n^2=k^2+[s+i\omega(\alpha+n)]/\nu, \tag{20}$$

which has the general solution

$$w_n(z)=P_n\cosh(kz)+Q_n\sinh(kz) \tag{21}$$

$$+R_n\cosh(q_n z)+S_n\sinh(q_n z). \tag{22}$$

The boundary conditions on w_n at the top surface, Eqs. (14) and (18), give

$$P_n=\nu(q_n^2+k^2)\zeta_n, \tag{23}$$

$$R_n=-2\nu k^2\zeta_n, \tag{24}$$

and the boundary conditions Eqs. (12) and (13) at the bottom surface give

$$Q_n=R\coth(q), \tag{25}$$

$$S_n=P\coth(k). \tag{26}$$

Finally, substitution of w_n into Eq. (15) yields

$$\nu^2\coth(q_n)k[(k^2+q_n^2)^2-4k^3q_n]\zeta_n=[-G(t)k^2\zeta]_n, \tag{27}$$

which will be transformed into an eigenvalue equation.

V. ACCELERATION OF THE LAYER AND THE INELASTIC BALL MODEL

For Faraday waves, $G(t)=1-\Gamma\cos(\omega t)$ so that the right hand side of Eq. (27) simply couples mode n to modes $n-1$ and $n+1$; the more complicated dynamics of the granular layer lead to a more complicated version of $G(t)$, as seen in Fig. 3. When the layer is in free flight, it feels no effects of

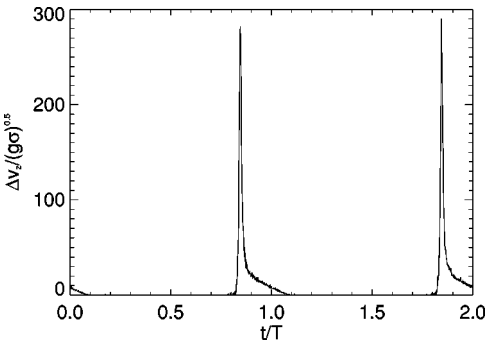

FIG. 3. Vertical momentum transfer from the bottom plate to particles per 1/1000 of a cycle. The momentum transfer is scaled with the gravitational acceleration and the particle diameter σ, while time is scaled with the oscillation period T. These data are from a simulation of 6000 particles at $\Gamma=2.1$, $H/\sigma=17$

gravity, when on the plate it feels $1-\Gamma\sin(\omega t)$, and when it hits the plate, it feels a strong acceleration. In the lab frame, the velocity of the layer is being rapidly changed from its negative downward velocity to the upward velocity of the plate.

We let

$$G(t)=\chi(t,t_{on},t_{off})[1-\Gamma\sin(\omega t)]+G^{\delta}(t,t_{on}), \quad (28)$$

where t_{on} and t_{off} are the times at which the layer makes and loses contact with the plate, $\chi(t,a,b)$ is equal to 1 for $a<t<b$ and 0 otherwise, and $G^{\delta}(t,t_{on})$ is a sharply peaked function at t_{on} that describes the acceleration of the layer due to the collision. Specifically, if the relative velocity between the plate and the layer is v_c, we model $G^{\delta}(t,t_{on})$ with

$$G^{\delta}(t,t_{on})=\frac{v_c}{\sqrt{\pi}\tau}e^{-[(t-t_{on})/\tau]^2}, \quad (29)$$

which integrated over time provides the impulse v_c to the layer. The parameter τ gives the width of the collisional spike, and is chosen to be $T/100$, where T is the period of oscillation. The values of t_{on}, t_{off}, and v_c are not given by the present theory; to get them we invoke the inelastic ball model [2]. According to this model, the layer effectively acts like a single particle with zero coefficient of restitution. It leaves the plate whenever the acceleration of the plate equals $-g$, so that t_{off} is defined from

$$-\Gamma\sin(\omega t_{off})=-1. \quad (30)$$

From that time, the inelastic particle travels parabolically until it strikes the plate at t_{on}:

$$z(t_{off})+v(t_{off})(t_{on}-t_{off})-(1/2)(t_{on}-t_{off})^2 = A\sin(\omega t_{on}), \quad (31)$$

where $z(t_{off})$ and $v(t_{off})$ are the height and velocity of the inelastic particle as it leaves the plate, and A is the dimensionless amplitude of the plate's oscillation. Equation (31) must be solved numerically for t_{on}. Finally, the collision velocity is the relative velocity between the plate and the ball when the two collide:

$$v_c=A\omega\cos(\omega t_{on})-v(t_{off})(t_{on}-t_{off}). \quad (32)$$

While the inelastic ball model oversimplifies the dynamics of the layer [3], bifurcations in the inelastic ball model closely correspond to experimentally observed bifurcations in the vibrated granular layer [4]. Further, these transitions depend only upon Γ, not upon ω, just as in experiment. This success justifies the supposition that the sequence of collisions is the determining factor in the stability of the flat state.

VI. DERIVATION OF THE EIGENVALUE EQUATION

Before expanding $G(t)$, we rewrite it as

$$G(t)=1+G^{\delta,\chi}+\Gamma G^{\Gamma}, \quad (33)$$

where

$$G^{\delta,\chi}=G^{\delta}-\chi(t,t_{on},t_{off}), \quad (34)$$

$$G^{\Gamma}=-\chi(t,t_{on},t_{off})\sin(\omega t). \quad (35)$$

Now, assume that each of these can be expanded into Fourier modes,

$$G^{\alpha}=\sum_l G_l^{\alpha}e^{i\omega l t}. \quad (36)$$

The products on the right hand side of Eq. (27), then, are

$$G^{\alpha}\zeta=\sum_n\sum_m G_{n-m}^{\alpha}\zeta_m e^{i\omega n t}. \quad (37)$$

Equation (27) becomes

$$A_{nm}\zeta_m=\Gamma B_{nm}\zeta_m, \quad (38)$$

where

$$A_{nm}=\delta_{nm}[1+(\nu^2/k)\coth(q_n)\{(k^2+q_n^2)^2-4k^3q_n\}] + G_{n-m}^{\delta,\chi}, \quad (39)$$

$$B_{nm}=-G_{n-m}^{\Gamma}. \quad (40)$$

To cast Eq. (38) as an eigenvalue problem, we must either invert A or B. In Refs. [10,11], A is inverted, since it is diagonal in the absence of $\Gamma^{\delta,\chi}$. Our A is more complicated, so instead we invert B. This inversion is simpler, because B is a Toeplitz matrix, i.e., the jth row of B is just the first row, shifted by j spaces [39]. Then,

$$M_{nm}\zeta_m=\Gamma\zeta_n, \quad (41)$$

where $M=B^{-1}A$.

VII. SOLUTION METHOD

In the fluid case, M is a function of s, α, k, ν, and ω. To find the critical Γ, s is set to 0, corresponding to marginal stability, and α to either 0 or 1/2. For a fixed ω, k is varied and the eigenvalues of M are found. This results in the marginal stability curve in the $\Gamma-k$ plane; the lowest point on this curve corresponds to the critical Γ and k for that frequency. Varying ω leads to the onset $\Gamma_c(\omega)$ and the disper-

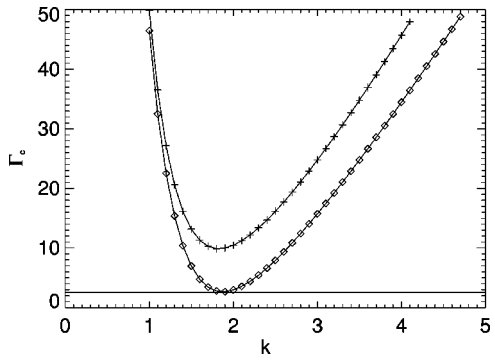

FIG. 4. Marginal stability curves, for $\omega=3.0$ and $+$: $\nu=0.2$, $\diamond$: $\nu=0.176$. Both calculations include 50 modes. The solid line is the consistency condition, $\Gamma_c=2.5$.

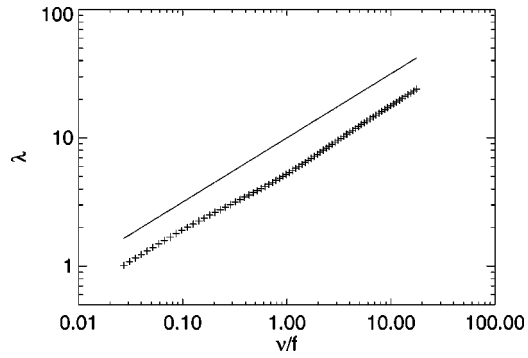

FIG. 5. Log-log plot of nondimensionalized wavelengths vs ν/f. The solid line has slope 1/2, corresponding to viscous wavelengths.

sion relation $k_c(\omega)$. Because the indices on M range from $-\infty$ to ∞, the expansion must be truncated, but because of the simple form of the acceleration for the fluid case, only a few modes must be kept to achieve accurate results.

In the granular case, the situation is somewhat less straightforward. M depends on not only s, α, k, ν, and ω, but also on ν_c, t_{on}, and t_{off}, which in turn depend on Γ. Furthermore, we don't know the viscosity ν for the granular layer, which will presumably depend in some way on the external control parameters Γ and ω.

Rather than taking ν as an input, and using it to calculate Γ_c and the dispersion relation, we will take Γ_c as a given, and use it to calculate ν and the dispersion relation. In experiments, the initial onset to patterns occurs near $\Gamma=2.5$. There is slight dependence on ω, but we will suppose that $\Gamma_c=2.5$ for all ω.

The critical ν and k will be functions of ω. For a given ω, we use the inelastic ball model to calculate t_{on}, t_{off}, and ν_c, assuming $\Gamma=2.5$. From these, the Fourier coefficients of the G^α are calculated; then A and B, assuming a given ν, and $s=0$ and $\alpha=1/2$, corresponding to marginal stability of subharmonic waves. The numerical recipe ctoeplz [39] inverts B, and calculates M. Then, the eigenvalues of M are calculated by the routine zgeev, a routine from the linear algebra package CLAPACK [40], which calculates the eigenvalues of a square nonsymmetric complex matrix.

These eigenvalues produce, by varying k, a marginal stability curve in the Γ-k plane; see Fig. 4. The lowest point on this curve again defines Γ_c. We have already assumed a given ν_c, t_{off}, and t_{on}, so that Γ_c is the acceleration amplitude between t_{off} and t_{on}. The physical condition that Γ_c be the same Γ that produced the parameters from the inelastic ball model now enters as an extra condition. To satisfy this condition, we vary ν until Γ_c is within 1% of the assumed critical Γ.

As in the fluid case, only a fixed number of modes are kept, but due to the rapidly varying G^δ, we must keep many more. Results with 30 modes and 50 modes differ by less that 1%, while results with 50 and 100 modes differ by less than one part in 10^4. For all subsequent results, we use $N=50$.

For Faraday waves at low frequencies, the response of the layer to oscillation may be harmonic, rather than subharmonic [11]. In experiments on granular media, only subharmonic response has been observed. To check for harmonic response in our analysis, we performed runs with $\alpha=0,1/2$, $\nu=1.41$, and $f=0.1$, which is the lowest frequency we investigate. Even for this low frequency, the critical acceleration for the onset of harmonic waves is a factor of 50 higher than that for subharmonic waves, so that only the subharmonic response must be studied for higher f.

VIII. RESULTS AND DISCUSSION

Figure 1 displays the dimensionless wavelength $\lambda=\lambda'/H$ as a function of dimensionless frequency $f=(\omega/2\pi)$ for experiment [17] at fixed $\Gamma=3.0$. On the same plot, the wavelengths of the most unstable mode $\lambda=2\pi/k_c$ for the model described above are shown. Given the amount of approximation involved in the model, the agreement is remarkable. At high and low frequencies the model systematically underestimates the wavelengths, suggesting that the functional form is probably incorrect, but note that no free parameters were used in fitting the data. The deviation at high frequency is probably not due to particle size effects, since for the deepest experimental layers in Fig. 1, the wavelengths are still about 60 particle diameters. The model predicts the most unstable wave number at onset, but Fig. 1 compares to data above onset, because those are the data available. Because the final state after a hysteretic transition is finite amplitude, comparison to a wavelength derived from linear theory may be misleading. However, experiments show that the wavelength depends only weakly upon Γ [17], which determines the distance above onset.

Because this model is isothermal, the dissipative properties of the granular media, assumed to be crucial in other continuum models, enter only indirectly. Rather, the formation of waves is opposed by the action of viscosity, as in the liquid case. As seen in Fig. 5, the wavelength in the model nearly scales as a viscous length, $\sqrt{\nu/f}$. As expected, the viscosity itself scales with the oscillation frequency; see Fig. 6. At low frequencies, $\nu\propto 1/f$; above $f\approx 0.45$, the scaling changes to $\nu\propto 1/f^3$. The wavelengths, then, scale as $1/f$ at low f, and cross over to $1/f^2$ for higher f.

Although indirect, the inelasticity of grains does play a role in the formation of these patterns. Inelasticity between grains causes a layer to condense, even in the absence of surface tension. Because collisions are inelastic, the layer as a whole is strongly inelastic in its interaction with the plate, approximating a single inelastic ball. Finally, the temperature

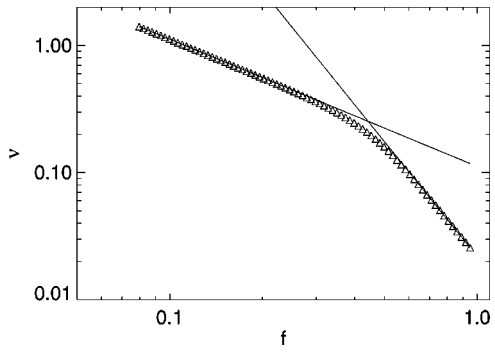

FIG. 6. Nondimensional log-log plot of viscosity vs frequency. The solid lines are fits to the high and low frequency regions and have slopes -3.0 and -1.0, respectively.

in the layer is controlled through a balance between production due to plate collision and loss due to inelasticity. The temperature controls the granular viscosity [24], which in turn controls the pattern wavelengths.

The low frequency scaling of the viscosity is consistent with kinetic theory ideas. The collision velocity scales with $Af \propto \Gamma/f$. At fixed Γ, $v_c \propto 1/f$. If we suppose that the average temperature scales with the collision velocity squared, and that the viscosity scales with $\sqrt{T}$, we find that $\nu \propto 1/f$. This argument relies on assuming that the average density of the layer is fixed as f varies, but this assumption is probably flawed. As frequency increases, the layer appears more compact.

The crossover at $f=0.45$ occurs when $\sqrt{\nu/f} \approx 1$, or when the dimensional viscous length, l_v', is approximately equal to the depth of the layer. Assuming that l_v' may depend upon H, g, and f', we find dimensionally that

$$l_v' \propto H^{\beta} g^{(1-\beta)} f' 2(\beta - 1), \tag{42}$$

where β cannot be determined with dimensional analysis. For low frequencies, $l_v' > H$, and the kinetic theory argument above implies $\beta = 1/2$. As the frequency increases, and l_v' becomes smaller than H, it also becomes independent of H. For $\beta = 0$, Eq. (42) implies that $\nu \propto f^{-3}$, which is the high frequency scaling.

From the outset, the model assumed that the granular layer was incompressible and isothermal, that the bottom surface remains flat, and that stress-free boundary conditions are reasonable. Any or all of these assumptions may be responsible for the deviations from experiment. However, the near agreement with experiment suggests that these effects are indeed of lesser importance, when compared to the timing and strength of the violent layer-plate collisions.

ACKNOWLEDGMENTS

We thank Harry Swinney for useful discussions and for a critical reading of this manuscript. C.B. also thanks H. Riecke and L. Tuckerman for interesting and useful discussions. This work was supported by the Engineering Research Program of the Office of Basic Energy Sciences of the Department of Energy.

[1] M. C. Cross and P. C. Hohenberg, Rev. Mod. Phys. **65**, 851 (1993).
[2] F. Melo, P. B. Umbanhowar, and H. L. Swinney, Phys. Rev. Lett. **75**, 3838 (1995).
[3] T. H. Metcalf, J. B. Knight, and H. M. Jaeger, Physica A **236**, 202 (1997).
[4] F. Melo, P. Umbanhowar, and H. L. Swinney, Phys. Rev. Lett. **72**, 172 (1994).
[5] A. Kudrolli and J. P. Gollub, Phys. Rev. D **97**, 133 (1996).
[6] D. Binks and W. van de Water, Phys. Rev. Lett. **78**, 4043 (1997).
[7] P. Umbanhowar, F. Melo, and H. L. Swinney, Nature (London) **382**, 793 (1996).
[8] O. Lioubashevski, H. Arbell, and J. Fineberg, Phys. Rev. Lett. **76**, 3959 (1996).
[9] O. Lioubashevski, Y. Hamiel, A. Agnon, Z. Reches, and J. Fineberg (unpublished).
[10] K. Kumar and L. S. Tuckerman, J. Fluid Mech. **279**, 49 (1994).
[11] K. Kumar, Proc. R. Soc. London, Ser. A **452**, 1113 (1996).
[12] J. Bechhoefer, V. Ego, S. Manneville, and B. Johnson, J. Fluid Mech. **288**, 325 (1995).
[13] L. Tsimring and I. Aronson, Phys. Rev. Lett. **79**, 213 (1997).
[14] D. H. Rothman, Phys. Rev. E **57**, R1239 (1998).
[15] E. Cerda, F. Melo, and S. Rica, Phys. Rev. Lett. **79**, 4570 (1998).
[16] E. Clément, L. Vanel, J. Rajchenbach, and J. Duran, Phys. Rev. E **53**, 2972 (1996).
[17] P. B. Umbanhowar, Ph.D. thesis, University of Texas at Austin, 1996.
[18] J. Eggers and H. Riecke, Phys. Rev. E **59**, 4476 (1999).
[19] C. Bizon, M. D. Shattuck, J. B. Swift, W. D. McCormick, and H. L. Swinney, Phys. Rev. Lett. **80**, 57 (1998).
[20] J. R. de Bruyn, C. Bizon, M. D. Shattuck, D. Goldman, J. B. Swift, and H. L. Swinney, Phys. Rev. Lett. **81**, 1421 (1998).
[21] C. L. Goodridge, W. T. Shi, H. G. E. Hentschel, and D. P. Lathrop, Phys. Rev. E **56**, 472 (1997).
[22] J. T. Jenkins and M. Shahinpoor, in *Mechanics of Granular Materials: New Models and Constitutive Relations*, edited by J. T. Jenkins and M. Satake (Elsevier Science Publishers B.V., Amsterdam, 1983), p. 339.
[23] C. K. K. Lun, S. B. Savage, D. J. Jeffrey, and N. Chepurniy, J. Fluid Mech. **140**, 223 (1983).
[24] J. T. Jenkins and M. W. Richman, Arch. Ration. Mech. Anal. **87**, 355 (1985).
[25] J. T. Jenkins and M. W. Richman, J. Fluid Mech. **192**, 313 (1988).
[26] A. Goldshtein and M. Shapiro, J. Fluid Mech. **282**, 75 (1995).
[27] C. Bizon, M. D. Shattuck, J. B. Swift, and H. L. Swinney, Phys. Rev. E **60**, 4340 (1999).
[28] J. T. Jenkins and S. B. Savage, J. Fluid Mech. **130**, 187 (1983).
[29] C. K. K. Lun and S. B. Savage, Acta Mech. **63**, 15 (1986).
[30] C. K. K. Lun, J. Fluid Mech. **233**, 539 (1991).
[31] T. G. Drake, J. Fluid Mech. **225**, 121 (1991).
[32] W. Losert, D. G. W. Cooper, J. Delour, A. Kudrolli, and J. P. Gollub, Chaos **9** (3), 682 (1999).

[33] J. S. Olafsen and J. S. Urbach, Phys. Rev. Lett. **81**, 4369 (1998).
[34] C. S. Campbell, Annu. Rev. Fluid Mech. **2**, 57 (1990).
[35] E. L. Grossman, T. Zhou, and E. Ben-Naim, Phys. Rev. E **55**, 4200 (1997).
[36] C. Bizon, Ph.D. thesis, University of Texas at Austin, 1998.
[37] C. Bizon, M. D. Shattuck, J. R. de Bruyn, J. B. Swift, W. D. McCormick, and H. L. Swinney, J. Stat. Phys. **93**, 449 (1998). Color pictures of granular convection can be found at http://chaos.ph.utexas.edu/errata/bizon98a.html.
[38] J. T. Jenkins, Trans. ASME, J. Appl. Mech. **59**, 120 (1992).
[39] W. H. Press, B. P. Flannery, S. A. Teukolsky, and W. T. Vetterling, *Numerical Recipes in C* (Cambridge University Press, Cambridge, 1988).
[40] E. Anderson, Z. Bai, C. Bischof, J. Demmel, J. Dongarra, J. Du Croz, A. Greenbaum, S. Hammarling, A. McKenney, S. Ostrouchov, and D. Sorensen, *LAPACK Users' Guide* 2nd ed. (Society for Industrial and Applied Mathematics, Philadelphia, PA, 1995).